

# Forced Oscillation Localization in Electric Power Systems under Resonance Conditions

Tong Huang, *Student Member, IEEE*, Nikolaos M. Freris, *Senior Member, IEEE*, P. R. Kumar, *Fellow, IEEE*, and Le Xie, *Senior Member, IEEE*

**Abstract**—This paper proposes a purely data-driven yet physically interpretable approach to locating the source of forced oscillations in cases where resonance phenomena arise. By leveraging the sparsity of the forced oscillation sources along with the low-rank nature of high-dimensional synchrophasor data, the problem of source localization under resonance conditions is cast as computing the sparse and low-rank components using Robust Principal Component Analysis (RPCA), which can be efficiently solved by the exact Augmented Lagrange Multiplier method. Built upon the RPCA-based problem formulation, an efficient and practically implementable algorithm is developed in order to pinpoint the forced oscillation source during online operation. Additionally, we provide theoretical insights into the efficacy of the proposed approach by use of physical model-based analysis, highlighting the fact that the rank of the resonance matrix is at most 2. The effectiveness of the proposed method is validated in the IEEE 68-bus power system and the WECC 179-bus benchmark system.

**Index Terms**—Forced oscillations, Phasor Measurement Unit (PMU), Resonant Systems, Robust Principal Component Analysis (RPCA), unsupervised learning, Big Data.

## I. INTRODUCTION

PHASOR measurement units (PMUs) enhance the transparency of bulk power systems by streaming the fast-sampled and synchronized measurements to system control centers. Such finely-sampled and time-stamped PMU measurements can reveal rich dynamical behaviors of the grid, which are invisible to the conventional supervisory control and data acquisition (SCADA) systems. These informative synchrophasor data are streamed to control centers in nearly real time, enabling system operators to detect, locate and mitigate system anomalies efficiently [1]–[4]. Among the system dynamical behaviors exposed by PMUs, *forced oscillations* (FO) have attracted significant attention within the power community. Forced oscillations are driven by periodically exogenous disturbances that are typically injected to power systems by malfunctioning power apparatuses [3], [5] such as wind turbines [6], [7], steam extractor valves of generators [8], or poorly-tuned control systems [9], [10]. Cyclic loads such as cement mills and steel plants, constitute another category of

oscillation sources [11]. The impact of such injected periodical perturbation propagates through transmission lines and results in forced oscillations throughout the grid; some real-world events of forced oscillations since 1966 are reported in [5].

The presence of forced oscillations compromises the security and reliability of power systems. For example, pronounced forced oscillations may trigger protection relays to trip transmission lines or generators, potentially causing uncontrollable cascading failures and unexpected load shedding [12]. Moreover, sustained forced oscillations reduce device lifespans by introducing undesirable vibrations and additional wear and tear on power system components; consequently, the failure rates and maintenance costs of the compromised power apparatuses might increase [12]. Therefore, timely suppression of forced oscillations is highly imperative for system operators.

One effective way to suppress a forced oscillation is to locate the oscillation's source, a canonical problem that we call *forced oscillation localization*, and to disconnect it from the power grid. Efficient localization is a key step in suppressing forced oscillations in the power grid. One might think that forced oscillation localization can be achieved by tracking the largest oscillation over the power grid, under the assumption that measurements near the oscillatory source will exhibit the most severe oscillations based on engineering intuition. However, counter-intuitive cases can occur when the frequency of the periodical perturbation lies in the vicinity of one of the natural modes of the power system, whence a *resonance phenomenon* is triggered [13]. In such cases, PMU measurements exhibiting the most severe oscillations may be geographically far from where the periodical perturbation is injected, posing a significant challenge to system operators in pinpointing the forced oscillation source. It is worth noting that such counter-intuitive cases are more than a mere theoretical concern: one example occurred at the Western Electricity Coordinating Council (WECC) system on Nov. 29, 2005, when a 20-MW forced oscillation initiated by a generation plant at Alberta incurred a tenfold larger oscillation at the California-Oregon Inter-tie line that is 1100 miles away from Alberta [8], [12]. Such an amplified oscillation significantly compromises the security and reliability of the power grid. Hence, it is necessary to develop a forced oscillation localization method that is effective even in the challenging but highly hazardous cases of resonance [3].

In order to pinpoint the source of forced oscillations, several localization techniques have been developed. In [14], forced oscillation localization is achieved based on the following observation: the measurements near the source manifest dis-

This work is supported in part by NSF Contracts ECCS-1760554, NSF CCF-1717207, NSF Science & Technology Center Grant CCF-0939370, and the Power Systems Engineering Research Center (PSERC).

T. Huang, P. R. Kumar and L. Xie are with the Departments of Electrical and Computer Engineering, Texas A&M University, College Station, TX 77843 USA (e-mail: tonghuang@tamu.edu; prk@tamu.edu; le.xie@tamu.edu).

N. Freris is with the School of Computer Science and Technology, University of Science and Technology of China, Hefei, Anhui, 230000 China (e-mail: nfreris2@gmail.com).

tinct signatures in their magnitude or phase responses, in comparison to far away measurements. Such an observation is interpretable based on classic generator models, but whether it is valid or not in a power system with complex generator dynamics remains an open question [14]. In addition, [9], [15], [16] leverage the oscillation energy flows in power networks to locate the source of sustained oscillations. In this energy-based method, the energy flows can be computed using the preprocessed PMU data [9] according to a formula derived in [15], and the power system components generating the oscillation energy are identified as the oscillation sources. In spite of the promising performance of the energy based method [9], the strong assumptions on load characteristics and the grid topology may restrict its usefulness to specific scenarios [3], [17]. In [18], the oscillation source is located by comparing the measured current spectrum of system components with one predicted by the effective admittance matrix. However, the construction of the effective admittance matrix requires accurate knowledge of system parameters that may be unavailable in practice. In [19], generator parameters are learned from measurements based on prior knowledge of generator model structures, and, subsequently, the admittance matrix is constructed and used for FO localization. Nevertheless, model structures of generators might not be known beforehand, owing to the unpredictable switching states of power system stabilizers [20]. Thus, it is highly desirable to design a FO localization method that does not heavily depend upon availability of the first-principle model and topology information of the power grid.

In this paper, we propose a *purely data-driven* yet *physically interpretable* approach to pinpoint the source of forced oscillations in the challenging resonance case. By leveraging the sparsity of the FO sources and the low-rank nature of high-dimensional synchrophasor data, the problem of forced oscillation localization is formulated as computing the sparse and low-rank components using Robust Principal Component Analysis (RPCA). Based on the problem formulation, an online algorithm is designed to pinpoint the source of forced oscillations. The main merits of the proposed approach include: 1) it does not require any information on dynamical system models and topology, thus enabling efficient and wide implementation in practice; 2) it can locate the source of forced oscillations with high accuracy, even when resonance phenomena occur; and 3) its efficacy can be interpreted by physical model-based analysis.

The rest of this paper is organized as follows: Section II elaborates on the forced oscillation localization problem and its main challenges; in Section III, the FO localization is formulated as a matrix decomposition problem and an online FO localization algorithm is designed; Section IV provides one theoretical interpretation for the algorithm's efficacy; Section V validates the effectiveness of the proposed method in the IEEE 68-bus power system and the WECC 179-bus power system; Section VI summarizes the paper and poses a future research question.

## II. LOCALIZATION OF FORCED OSCILLATIONS AND CHALLENGES

### A. Mathematical Interpretation

The dynamic behavior of a power system in the vicinity of its operation condition can be represented by a continuous linear time-invariant (LTI) state-space model [4], [21]:

$$\dot{\mathbf{x}}(t) = \mathbf{A}\mathbf{x}(t) + \mathbf{B}\mathbf{u}(t) \quad (1a)$$

$$\mathbf{y}(t) = \mathbf{C}\mathbf{x}(t) \quad (1b)$$

where state vector  $\mathbf{x} \in \mathbb{R}^n$ , input vector  $\mathbf{u} \in \mathbb{R}^r$ , and output vector  $\mathbf{y} \in \mathbb{R}^m$  collect the *deviations* of state variables, generator/load control setpoints, and measurements from their respective steady-state values. Accordingly, matrices  $\mathbf{A} \in \mathbb{R}^{n \times n}$ ,  $\mathbf{B} \in \mathbb{R}^{n \times r}$  and  $\mathbf{C} \in \mathbb{R}^{m \times n}$  are termed as the state matrix, the input matrix and the output matrix, respectively. Denote by  $\mathcal{L} = \{\lambda_1, \lambda_2, \dots, \lambda_n\}$  the set of all eigenvalues of the state matrix  $\mathbf{A}$ . The power system (1) is assumed to be stable, with all eigenvalues  $\lambda_i \in \mathbb{C}$  being distinct, i.e.,  $\text{Re}\{\lambda_i\} < 0$  for all  $i \in \{1, 2, \dots, n\}$  and  $\lambda_i \neq \lambda_j$  for all  $i \neq j$ .

We proceed to rigorously define a forced oscillation source as well as source measurements. Suppose that the  $l$ -th input  $u_l(t)$  in the input vector  $\mathbf{u}(t)$  varies periodically due to malfunctioning components (generators/loads) in the grid. In such case,  $u_l(t)$  can be decomposed into  $F$  frequency components, viz.,

$$u_l(t) = \sum_{j=1}^F P_j \sin(\omega_j t + \theta_j), \quad (2)$$

where  $\omega_j \neq 0$ ,  $P_j \neq 0$  and  $\theta_j$  are the frequency, amplitude and phase displacement of the  $j$ -th frequency component of the  $l$ -th input, respectively. As a consequence, the periodical input will result in sustained oscillations in the measurement vector  $\mathbf{y}$ . The generator/load associated with input  $l$  is termed as the *forced oscillation source*, and the measurements at the bus directly connecting to the forced oscillation source are termed as *source measurements*.

In particular, suppose that the frequency  $\omega_d$  of an injection component is close to the frequency of a poorly-damped mode, i.e., there exists  $j^* \in \{1, 2, \dots, n\}$ ,

$$\omega_d \approx \text{Im}\{\lambda_{j^*}\}, \quad \text{Re}\{\lambda_{j^*}\}/|\lambda_{j^*}| \approx 0. \quad (3)$$

In such case, oscillations with growing amplitude, i.e., resonance, may be observed [13], [22]. Hence, (3) is adopted as *resonance condition* in this paper.

In a power system with PMUs, the measurement vector  $\mathbf{y}(t)$  is sampled at  $f_s$  times in each second. Within a time interval from the FO starting point up to time instant  $t$ , the time evolution of the measurement vector  $\mathbf{y}(t)$  can be discretized by sampling and represented by a matrix called a *measurement matrix*  $Y_t = [y_{p,q}^t]$ , which we formally define next. Denote by zero the time instant when the forced oscillations start. The following column concatenation defines the measurement matrix  $Y_t$  up to time  $t$ :

$$Y_t := [\mathbf{y}(0) \quad \mathbf{y}(1/f_s) \quad \dots \quad \mathbf{y}(n/f_s) \quad \dots \quad \mathbf{y}(\lfloor t f_s \rfloor / f_s)], \quad (4)$$

where  $\lfloor \cdot \rfloor$  is the floor operation. The  $i$ -th column of the measurement matrix  $Y_t$  in (4) suggests the “snapshot” of all synchrophasor measurements over the system at the time  $(i-1)/f_s$ . The  $k$ -th row of  $Y_t$  denotes the time evolution of the  $k$ -th measurement deviation in the output vector  $y$ .

The forced oscillation localization is equivalent to pinpointing the forced oscillation source using measurement matrix  $Y_t$ . Due to the complexity of power system dynamics, the precise power system model (1) may not be available to system operators during real-time operation. Therefore, it is assumed that the only known information for forced oscillation localization is the measurement matrix  $Y_t$ . In brief, the first-principle model (1) as well as the perturbation information (2) is introduced mainly for the purpose of defining FO localization problem and theoretically justifying the data-driven method proposed in Section III.

### B. Main Challenges of Pinpointing the Sources of Forced Oscillation

The topology of the power system represented by (1) can be characterized by an undirected graph  $G(\mathcal{B}, \mathcal{T})$ , where vertex set  $\mathcal{B}$  comprises all buses in the power system, while edge set  $\mathcal{T}$  collects all transmission lines. Suppose that the PMU measurements at bus  $i^* \in \mathcal{B}$  are the source measurements. Then bus  $j^*$  is said to be in the vicinity of the FO source, if bus  $j^*$  is a member of the following vicinity set

$$\mathcal{V} = \{j \in \mathcal{B} | d_G(i^*, j) \leq N_0\} \quad (5)$$

where  $d_G(i, j)$  denotes the  $i$ - $j$  distance, viz., the number of transmission lines (edges) in a shortest path connecting buses (vertices)  $i$  and  $j$  [23]; the threshold  $N_0$  is a nonnegative integer. In particular,  $\mathcal{V} = \{i^*\}$  for the source measurement at bus  $i^*$ , if  $N_0$  is set to zero.

Intuitively, one may suppose that the source measurement can be localized by finding the maximal absolute element in the measurement matrix  $Y_t$ , based on the intuition that the most severe oscillation should be manifested in the vicinity of the source. However, a major challenge for pinpointing the FO sources arises from the following (counter-intuitive) fact: the most severe oscillation does not necessarily manifest near the FO source, in the presence of the resonance phenomena. Following the same notation as in (4) and (5), we term a measurement matrix  $Y_t$  as the *counter-intuitive case*, if

$$p^* \notin \mathcal{V}, \quad (6)$$

where  $p^*$  can be obtained by finding the row index of the maximal element in the measurement matrix  $Y_t$ , i.e.,

$$[p^*, q^*] = \arg \max_{p,q} y_{p,q}^t. \quad (7)$$

It is such counter-intuitive cases that make pinpointing the FO source challenging [13]. Figure 1 illustrates one such counter-intuitive case, where the source measurement (red) is not the most severe oscillation. Additional examples of counter-intuitive cases can be found in [3]. Although the counter-intuitive cases are much less likely to happen than the intuitive ones in terms of rarity of occurrence, it is still imperative to design an algorithm to pinpoint the FO source even in the

counter-intuitive cases due to the hazardous consequences of the forced oscillations under resonance conditions.

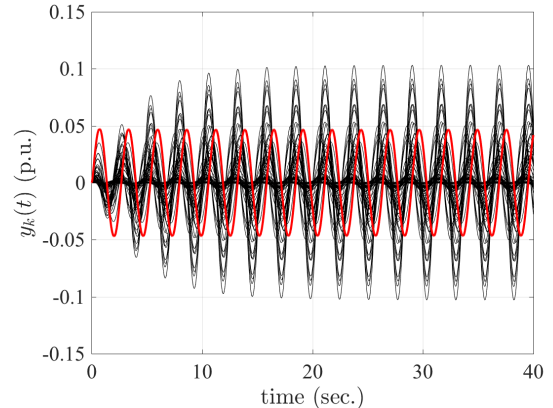


Fig. 1. One counter-intuitive case [3] the IEEE 68-bus benchmark system [24]: the black curves correspond to the non-source measurements; the red curve corresponds to the source measurement.

## III. PROBLEM FORMULATION AND PROPOSED METHODOLOGY

In this section, we first formulate the FO localization problem as a matrix decomposition problem. Then, an empirical explanation for the formulation is followed. Finally, we present a FO localization algorithm for online operation.

### A. Problem Formulation

Given a measurement matrix  $Y_t$  up to time  $t$ , the FO source localization is formulated as decomposing the measurement matrix  $Y_t$  into a low-rank matrix  $L_t$  and a sparse matrix  $S_t$ :

$$Y_t = L_t + S_t \quad (8a)$$

$$\text{rank } L_t \leq \alpha \quad (8b)$$

$$\|S_t\|_0 \leq \beta, \quad (8c)$$

where the pseudo-norm  $\|\cdot\|_0$  returns the number of non-zero elements of a matrix; the non-negative integer  $\alpha$  is the upper bound of the rank of the low-rank matrix  $L_t$ , and the non-negative integer  $\beta$  is the upper bound on the number of non-zero entries in the sparse matrix  $S_t$ . Given non-negative integers  $\alpha$  and  $\beta$ , it is possible to numerically find  $\{L_t, S_t\}$  via *alternating projections* [3].

Next, we offer an empirical explanation for the problem formulation in (8). The spatial correlation among PMU measurements resulting from the tight electrical coupling between buses contributes an underlying low-rank structure of the measurement matrix  $Y_t$ . The low-rank nature of  $Y_t$  is due to the “general trend” of PMU measurements in the time domain [3]. The source measurements are expected to deviate from the “general trend” the most, and such deviation is supposed to be captured by the discrepancy between the measurement matrix  $Y_t$  and the low-rank component. Owing to the limited number of source measurements, we expect the discrepancy matrix  $S_t$  to be a sparse matrix. The low-rank and sparse components are assumed to be captured by matrices  $L_t = [l_{p,q}^t]$  and

$S_t = [s_{p,q}^t]$ , respectively. The source measurement index  $i^*$  can be tracked by finding the largest absolute value in the sparse matrix  $S_t$ , viz.,

$$[p^*, q^*]^\top = \arg \max_{p,q} |s_{p,q}^t|. \quad (9)$$

Due to the non-convexity of (8) and the prior unavailability of the upper bounds  $\alpha$  and  $\beta$  [3], the matrix deposition problem shown in (8) is reformulated as a instance of Robust Principal Component Analysis (RPCA) problem:

$$\min_{S_t} \|Y_t - S_t\|_* + \xi \|S_t\|_1, \quad (10)$$

where  $\|\cdot\|_*$  and  $\|\cdot\|_1$  denote the nuclear norm and  $l_1$  norm, respectively; the tunable parameter  $\xi$  regulates the extent of the sparsity of  $S_t$ . The formulation in (10) is a convex relaxation of (8). Under some assumptions, the sparse matrix  $S_t$  and the low-rank matrix  $L_t$  can be disentangled from the measurement matrix  $Y_t$  [25] by diverse algorithms [26]. The exact Lagrange Multiplier Method (ALM) is used to solve the formulation (10) in this paper.

### B. Online FO Localization Algorithm

Next, we present an FO localization algorithm for online operation, using the formulation (10). The starting point of forced oscillations can be determined by the event detector and classifier reported in [2], [27]–[29]. Once the starting point of forced oscillations is detected, the forced oscillation source can be pinpointed by Algorithm 1, where  $T_0$  and  $\xi$  are user-defined parameters.

---

#### Algorithm 1 Real-time FO Localization

---

- 1: Update  $Y_{T_0}$  by (4);
  - 2: Find  $S_t$  in (10) via the exact ALM for chosen  $\xi$ ;
  - 3: Obtain  $p^*$  by (9);
  - 4: **return**  $p^*$  as the source measurement index.
- 

## IV. THEORETICAL INTERPRETATION OF THE RPCA-BASED ALGORITHM

This section aims to develop a theoretical connection between the first-principle model in Section II and the data-driven approach presented in Section III. We start such an investigation by deriving the time-domain solution to PMU measurements in a power system under resonance conditions. Then, the resonance matrix for the power grid is obtained from the derived solution to PMU measurements. Finally, the efficacy of the proposed method is interpreted by examining the rank of the resonance matrix.

### A. PMU Measurement Decomposition

For the power system with  $r$  inputs and  $m$  PMU measurements modeled in (1), the  $k$ -th measurement and the  $l$ -th input can be related by

$$\dot{\mathbf{x}}(t) = \mathbf{A}\mathbf{x}(t) + \mathbf{b}_l u_l(t) \quad (11a)$$

$$y_k(t) = \mathbf{c}_k \mathbf{x}(t), \quad (11b)$$

where column vector  $\mathbf{b}_l \in \mathbb{R}^n$  is the  $l$ -th column of matrix  $B$  in (1), and row vector  $\mathbf{c}_k \in \mathbb{R}^n$  is the  $k$ -th row of matrix  $C$ . Let  $\mathbf{x} = M\mathbf{z}$ , where  $\mathbf{z}$  denotes the transformed state vector and matrix  $M$  is chosen such that the similarity transformation of  $A$  is diagonal, then

$$\dot{\mathbf{z}}(t) = \mathbf{\Lambda}\mathbf{z}(t) + M^{-1}\mathbf{b}_l u_l(t) \quad (12a)$$

$$y_k(t) = \mathbf{c}_k M\mathbf{z}(t), \quad (12b)$$

where  $\mathbf{\Lambda} = \text{diag}(\lambda_1, \lambda_2, \dots, \lambda_n) = M^{-1}AM$ . Denote by column vector  $\mathbf{r}_i \in \mathbb{C}^n$  and row vector  $\mathbf{l}_i \in \mathbb{C}^n$  the right and left eigenvectors associated with the eigenvalue  $\lambda_i$ , respectively. Accordingly, the transformation matrices  $M$  and  $M^{-1}$  can be written as  $[\mathbf{r}_1, \mathbf{r}_2, \dots, \mathbf{r}_n]$  and  $[\mathbf{l}_1^\top, \mathbf{l}_2^\top, \dots, \mathbf{l}_n^\top]^\top$ , respectively. The transfer function in the Laplace domain from  $l$ -th input to  $k$ -th output is

$$\begin{aligned} H(s) &= \mathbf{c}_k M (sI - \mathbf{\Lambda})^{-1} M^{-1} \mathbf{b}_l \\ &= \sum_{i=1}^n \frac{\mathbf{c}_k \mathbf{r}_i \mathbf{l}_i \mathbf{b}_l}{s - \lambda_i}. \end{aligned} \quad (13)$$

For simplicity, assume that the periodical injection  $u_l$  only contains one component with frequency  $\omega_d$  and amplitude  $P_d$ , namely,  $F = 1$ ,  $\omega_1 = \omega_d$  and  $P_1 = P_d$  in (2). Furthermore, we assume that, before  $t = 0^-$ , the system is in steady state, viz.,  $\mathbf{x}(0^-) = \mathbf{0}$ . Let sets  $\mathcal{N}$  and  $\mathcal{M}'$  collect the indexes of real eigenvalues and the indexes of complex eigenvalues with positive imaginary parts, respectively, viz.,

$$\mathcal{N} = \{i \in \mathbb{Z}^+ | \lambda_i \in \mathbb{R}\}; \quad \mathcal{M}' = \{i \in \mathbb{Z}^+ | \text{Im}(\lambda_i) > 0\}. \quad (14)$$

Then the Laplace transform for the PMU measurement  $y_k$  is

$$\begin{aligned} Y_k(s) &= \left( \sum_{i=1}^n \frac{\mathbf{c}_k \mathbf{r}_i \mathbf{l}_i \mathbf{b}_l}{s - \lambda_i} \right) \frac{P_d \omega_d}{s^2 + \omega_d^2} \\ &= \left[ \sum_{i \in \mathcal{N}} \frac{\mathbf{c}_k \mathbf{r}_i \mathbf{l}_i \mathbf{b}_l}{s - \lambda_i} + \sum_{i \in \mathcal{M}'} \left( \frac{\mathbf{c}_k \mathbf{r}_i \mathbf{l}_i \mathbf{b}_l}{s - \lambda_i} + \frac{\mathbf{c}_k \bar{\mathbf{r}}_i \bar{\mathbf{l}}_i \mathbf{b}_l}{s - \bar{\lambda}_i} \right) \right] \frac{P_d \omega_d}{s^2 + \omega_d^2} \end{aligned} \quad (15)$$

where  $\bar{(\cdot)}$  denotes complex conjugation.

Next, we analyze the components resulting from the real eigenvalues and the components resulting from the complex eigenvalues individually.

1) *Components resulting from real eigenvalues:* In the Laplace domain, the component resulting from a real eigenvalue  $\lambda_i$  is

$$Y_{k,i}^D(s) = \frac{\mathbf{c}_k \mathbf{r}_i \mathbf{l}_i \mathbf{b}_l}{s - \lambda_i} \frac{P_d \omega_d}{s^2 + \omega_d^2}. \quad (16)$$

The inverse Laplace transform of  $Y_{k,i}^D(s)$  is

$$y_{k,i}^D(t) = \frac{\mathbf{c}_k \mathbf{r}_i \mathbf{l}_i \mathbf{b}_l P_d \omega_d}{\lambda_i^2 + \omega_d^2} e^{\lambda_i t} + \frac{\mathbf{c}_k \mathbf{r}_i \mathbf{l}_i \mathbf{b}_l P_d}{\sqrt{\lambda_i^2 + \omega_d^2}} \sin(\omega_d t + \phi_{i,l}) \quad (17)$$

where

$$\phi_{i,l} = \angle \left( \sqrt{\lambda_i^2 + \omega_d^2} + j\lambda_i \right)$$

and  $\angle(\cdot)$  denotes the angle of a complex number.

2) *Components resulting from complex eigenvalues:* In the Laplace domain, the component resulting from a complex eigenvalue  $\lambda_i = -\sigma_i + j\omega_i$  is

$$Y_{k,i}^B(s) = \left( \frac{\mathbf{c}_k \mathbf{r}_i \mathbf{l}_i \mathbf{b}_l}{s - \lambda_i} + \frac{\mathbf{c}_k \bar{\mathbf{r}}_i \bar{\mathbf{l}}_i \mathbf{b}_l}{s - \bar{\lambda}_i} \right) \frac{P_d \omega_d}{s^2 + \omega_d^2}. \quad (18)$$

The inverse Laplace transform of  $Y_{k,i}^B(s)$  is

$$\begin{aligned} y_{k,i}^B(t) = & \frac{2P_d \omega_d |\mathbf{c}_k \mathbf{r}_i \mathbf{l}_i \mathbf{b}_l|}{\sqrt{(\sigma_i^2 + \omega_d^2 - \omega_i^2)^2 + 4\omega_i^2 \sigma_i^2}} e^{-\sigma_i t} \cos(\omega_i t + \theta_{k,i} - \psi_i) + \\ & \frac{2P_d |\mathbf{c}_k \mathbf{r}_i \mathbf{l}_i \mathbf{b}_l| \sqrt{\omega_d^2 \cos^2 \theta_{k,i} + (\sigma_i \cos \theta_{k,i} - \omega_i \sin \theta_{k,i})^2}}{\sqrt{(\sigma_i^2 - \omega_d^2 + \omega_i^2)^2 + 4\omega_d^2 \sigma_i^2}} \times \\ & \cos(\omega_d t + \phi_i - \alpha_i), \end{aligned} \quad (19)$$

where

$$\theta_{k,i} = \angle(\mathbf{c}_k \mathbf{r}_i \mathbf{l}_i \mathbf{b}_l), \quad (20)$$

$$\psi_i = \angle(\sigma_i^2 + \omega_d^2 - \omega_i^2 - j2\sigma_i \omega_i), \quad (21)$$

$$\phi_i = \angle(\sigma_i^2 - \omega_d^2 + \omega_i^2 - j2\omega_i \sigma_i), \text{ and} \quad (22)$$

$$\alpha_i = \angle[\omega_d \cos \theta_{k,i} + j(\sigma_i \cos \theta_{k,i} - \omega_i \sin \theta_{k,i})]. \quad (23)$$

3) *Resonance component:* Under the resonance condition defined in (3), the injection frequency  $\omega_d$  is in the vicinity of one natural modal frequency  $\omega_{j^*}$ , and the real part of the natural mode is small. We define a new set  $\mathcal{M} \subset \mathcal{M}'$  as follows:

$$\mathcal{M} = \{i \in \mathbb{Z}^+ \mid \text{Im}(\lambda_i) > 0, |\omega_i - \omega_{j^*}| > \kappa\}, \quad (24)$$

where  $\kappa$  is a small and nonnegative real number.

For  $i \notin \mathcal{M} \cup \mathcal{N}$ , the eigenvalue  $\lambda_i = -\sigma_i + j\omega_i$  satisfies

$$\omega_i \approx \omega_{j^*} \approx \omega_d; \quad \sigma_i \approx 0. \quad (25)$$

Then, according to Equations (20) to (23),

$$\psi_i \approx -\frac{\pi}{2}; \quad \phi_i \approx -\frac{\pi}{2}; \quad \alpha_i \approx -\theta_{k,i}. \quad (26)$$

Finally, equation (19) can be simplified as

$$y_{k,i}^B(t) \approx y_{k,i}^R(t) = \frac{P_d |\mathbf{c}_k \mathbf{r}_i \mathbf{l}_i \mathbf{b}_l|}{\sigma_i} (1 - e^{-\sigma_i t}) \sin(\omega_d t + \theta_{k,i}) \quad (27)$$

for  $i \notin \mathcal{M} \cup \mathcal{N}$ . In this paper,  $y_{k,i}^R$  in (27) is termed as the *resonance component* in the  $k$ -th measurement.

In summary, a PMU measurement  $y_k(t)$  in a power system (1) under resonance conditions can be decomposed into three categories of components, i.e.,

$$y_k(t) = \sum_{i \in \mathcal{N}} y_{k,i}^D(t) + \sum_{i \in \mathcal{M}} y_{k,i}^B(t) + \sum_{i \notin \mathcal{M} \cup \mathcal{N}} y_{k,i}^R(t). \quad (28)$$

*B. Observations on the resonance component and the resonance-free component*

1) *Severe oscillations arising from resonance component:*

Figure 2 visualizes the resonance component of a PMU measurement in the IEEE 68-bus benchmark system. As can be observed in Figure 2, the upper envelop of the oscillation increases concavely at the initial stage before reaching a steady-stage value (about 0.1 in this case). The close-form approximation for such a steady-state value is  $P_d |\mathbf{c}_k \mathbf{r}_i \mathbf{l}_i \mathbf{b}_l| / \sigma_i$ . For a small positive  $\sigma_{j^*}$  associated with eigenvalue  $\lambda_{j^*}$ , the steady-state amplitude of the resonance component may be the dominant one. If a PMU measurement far away from the source measurements is tightly coupled with the eigenvalue  $\lambda_{j^*}$ , it may manifest the most severe oscillation, thereby confusing system operators in terms of FO source localization. Therefore, the presence of resonance components may cause the counter-intuitive cases defined by (6), (7).

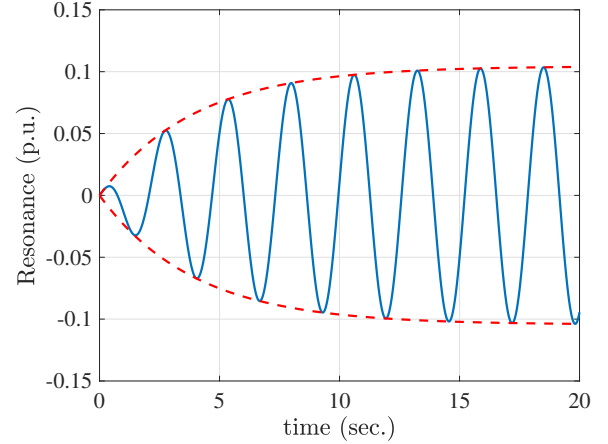


Fig. 2. Visualization of the resonance component of a PMU measurement in the IEEE 68-bus benchmark system based on equation (27): the resonance components of the bus magnitude measurement at Bus 40 (blue curve) and its envelopes (red-dash curves).

2) *Location information on FO source from the resonance-free component:* As the resonance components of the set of all PMU measurements mislead system operators with respect to FO localization, it may be interesting to exclude the resonance component from (28), and to check if the remaining components exhibit any spatial information concerning the FO source. The superposition of the remaining components is termed as *resonance-free*. For a power system with known physical model (1), the resonance-free component  $y_k^F$  in the  $k$ -th PMU measurement time series can be obtained by

$$y_k^F(t) = \sum_{i \in \mathcal{N}} y_{k,i}^D(t) + \sum_{i \in \mathcal{M}} y_{k,i}^B(t). \quad (29)$$

The visualization of the resonance-free component for all PMU measurements in the IEEE 68-bus system is shown in Figure 3 under a certain FO setting<sup>1</sup>. Under the same FO setting, Figure 1 visualizes all PMU measurements  $y_k(t)$  in

<sup>1</sup>A sinusoidal waveform with amplitude 0.05 p.u. and frequency 0.38 Hz is injected into the IEEE 68-bus system via the voltage setpoint of generator 13. The information of the test system is elaborated in Section V.

(28). While the complete measurements  $y_k(t)$  are counter-intuitive in Figure 1, the resonance-free components  $y_k^F(t)$  convey the location information on the FO source in Figure 3—the resonance-free component of the source measurement exhibits the largest oscillation.

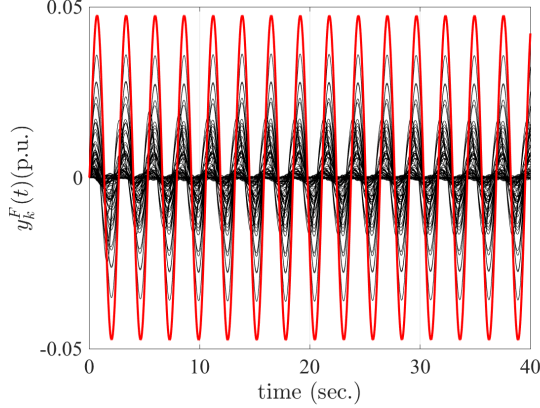


Fig. 3. Resonance-free components of the source measurement (red) and the non-source measurement (black) in the IEEE 68-bus benchmark system.

### C. Low-rank Nature of Resonance Matrix

The physical interpretation of the RPCA-based method can be pushed forward by examining the rank of the matrix containing all resonance components for all measurements, which we call the *resonance matrix* formally defined next. Similar to (4), the resonance component  $y_k^R(t)$  in the  $k$ -th measurement can be discretized into a row vector  $\mathbf{y}_{k,t}^R$ :

$$\mathbf{y}_{k,t}^R := [y_k^R(0) \quad y_k^R(1/f_s) \quad \dots \quad y_k^R(\lfloor tf_s \rfloor / f_s)]. \quad (30)$$

Then, the resonance matrix  $Y_t^R$  can be defined as a row concatenation as follows:

$$Y_t^R := \left[ (\mathbf{y}_{1,t}^R)^\top \quad (\mathbf{y}_{2,t}^R)^\top \quad \dots \quad (\mathbf{y}_{m,t}^R)^\top \right]^\top. \quad (31)$$

**Theorem 1.** *For the linear time-invariant dynamical system (1), the rank of the resonance matrix  $Y_t^R$  defined in (31) is at most 2.*

*Proof.* Based on (27),

$$E_k := P_d |\mathbf{c}_k \mathbf{r}_i \mathbf{l}_i \mathbf{b}_l| / \sigma_i. \quad (32)$$

Then

$$y_k^R(t) = (1 - e^{-\sigma t}) \sin(\omega_d t) E_k \cos(\theta_{k,i}) + (1 - e^{-\sigma t}) \cos(\omega_d t) E_k \sin(\theta_{k,i}).$$

Define functions  $f_1(t)$ ,  $f_2(t)$  and variables  $g_1(k)$ ,  $g_2(k)$  as follows:

$$f_1(t) := (1 - e^{-\sigma t}) \sin(\omega_d t); \quad f_2(t) := (1 - e^{-\sigma t}) \cos(\omega_d t);$$

$$g_1(k) := E_k \cos(\theta_{k,i}); \quad g_2(k) := E_k \sin(\theta_{k,i}).$$

Then,  $y_k^R(t)$  can be represented by

$$y_k^R(t) = f_1(t)g_1(k) + f_2(t)g_2(k). \quad (33)$$

Based on (30), (31) and (33), the resonance matrix  $Y_t^R$  up to time  $t$  can be factorized as follows:

$$Y_t^R = \begin{bmatrix} g_1(1) & g_2(1) \\ g_1(2) & g_2(2) \\ \vdots & \vdots \\ g_1(m) & g_2(m) \end{bmatrix} \begin{bmatrix} f_1(0) & f_1(\frac{1}{f_s}) & \dots & f_1(\frac{\lfloor tf_s \rfloor}{f_s}) \\ f_2(0) & f_2(\frac{1}{f_s}) & \dots & f_2(\frac{\lfloor tf_s \rfloor}{f_s}) \end{bmatrix}. \quad (34)$$

Denote by vectors  $\mathbf{g}_1$  and  $\mathbf{g}_2$  the first and second columns of the first matrix in the right hand side (RHS) of (34), respectively; and by vectors  $\mathbf{f}_1$  and  $\mathbf{f}_2$  the first and second rows of the second matrix in the RHS of (34). Then (34) turns to be

$$Y_t^R = [\mathbf{g}_1 \quad \mathbf{g}_2] \begin{bmatrix} \mathbf{f}_1 \\ \mathbf{f}_2 \end{bmatrix}. \quad (35)$$

Given (35), it becomes clear that the rank of the resonance matrix  $Y_t^R$  is at most 2.  $\square$

Typically, for a resonance matrix  $Y_t^R$  with  $m$  rows and  $\lfloor tf_s \rfloor$  columns, owing to  $\min(m, \lfloor tf_s \rfloor) \gg 2$ , the resonance matrix  $Y_t^R$  is a low-rank matrix, which is assumed to be captured by the low-rank component  $L_t$  in equation (8). As discussed in Section IV-B2, the source measurement can be tracked by finding the maximal absolute entry of the resonance-free matrix  $(Y_t - Y_t^R)$ . According to (9), the PMU measurement containing the largest absolute entry in the sparse component  $S_t$  is considered as the source measurement. Then, it is reasonable to conjecture that the sparse component  $S_t$  in (8) captures the part of the resonance-free matrix that preserves the location information of FO source. Therefore, a theoretical connection between the proposed data-driven method in Algorithm 1 and the physical model of power systems described in equation (1) is established.

## V. CASE STUDY

In this section, we validate the effectiveness of Algorithm 1 using data from two benchmark power systems. As will be seen, the proposed method can pinpoint the FO sources with high accuracy, even when resonance exists.

### A. Performance Validation of the Source Localization Method in the IEEE 68-bus System

In this subsection, the performance of Algorithm 1 is validated by the IEEE 68-bus benchmark system. We first describe the key information on the test system. Then the procedure for creating the counter-intuitive cases defined in Section II-B is demonstrated in detail. Finally, focusing on the obtained counter-intuitive cases, the performance of the proposed algorithm is tested and analyzed.

#### 1) System Description of the IEEE 68-bus Power System:

The system parameters of the IEEE 68-bus power system are reported in the Power System Toolbox (PST) [24] and its topology is shown in Figure 4. Let  $\mathcal{V} = \{1, 2, \dots, 16\}$  consist of the indexes of all 16 generators in the 68-bus system. Based on the original parameters, the following modifications are made: 1) the power system stabilizers (PSS) at all generators, except the one at Generator 9, are removed, in order to

create more poorly-damped oscillatory modes; 2) for the PSS at Generator 9, the product of PSS gain and washout time constant is changed to 250. Based on the modified system, the linearized model of the power system (1) can be obtained by command “svm\_mgen” in PST. There are 25 oscillatory modes whose frequencies range from 0.1 Hz to 2 Hz. Denote by  $\mathcal{W} = \{\omega_1, \omega_2, \dots, \omega_{25}\}$  the set consisting all 25 modal frequencies of interest. The periodical perturbation  $u_l$  in (2) is introduced through the voltage setpoints of generators. The analytical expression of  $u_l$  is  $0.05 \sin(\omega_d t)$ , where  $\omega_d \in \mathcal{W}$ . The bus voltage magnitude deviations constitute the output/measurement vector  $\mathbf{y}(t)$  in (1).

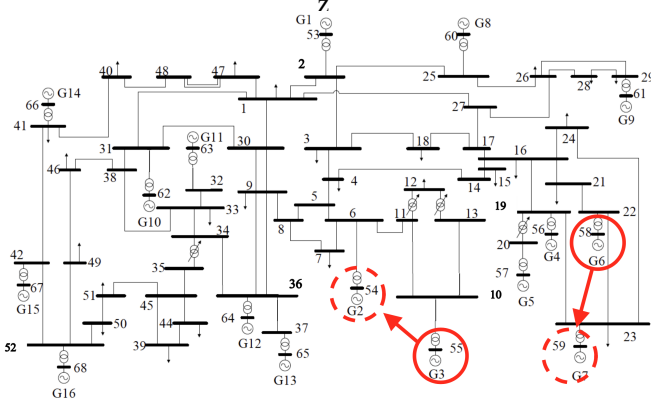


Fig. 4. The IEEE 68-bus power system [3], [30]: the generator in the solid circle is the actual source generators; the generator in the dash circle is the identified source.

2) *Synthesis of counter-intuitive cases*: We create forced oscillations in the 68-bus system according to set  $\mathcal{V} \times \mathcal{W}$ . For element  $(i, \omega_j) \in \mathcal{V} \times \mathcal{W}$ , the periodical perturbation  $u_l(t)$  with frequency  $\omega_j$  is injected into the grid through the voltage setpoint of generator  $i$  at time  $t = 0$ . Then, the system response is obtained by conducting a 40-second simulation. Finally, the measurement matrix is constructed based on (4), where the sampling rate  $f_s$  is 60 Hz. By repeating the above procedure for each element in set  $\mathcal{V} \times \mathcal{W}$ , we obtain 400 measurement matrices ( $|\mathcal{V} \times \mathcal{W}|$ ). For the 400 measurement matrices, 44 measurement matrices satisfy the resonance criteria (6), (7) with  $N_0 = 0$  and they are marked as the counter-intuitive cases which are used for testing the performance of the proposed method.

3) *Algorithm settings and simulation results for the IEEE 68-bus power system*: The tunable parameters  $T_0$  and  $\xi$  in Algorithm 1 are set to 10 and 0.0408, respectively. The detailed information on setting  $\xi$  can be found in [26]. Then, we apply Algorithm 1 for the 44 counter-intuitive cases. Algorithm 1 can pinpoint the source measurements in 40 counter-intuitive cases and, therefore, achieves 90.91% accuracy without any knowledge of system models and grid topology.

Next, we scrutinize the geographic proximity between the identified and actual source measurements in the 4 failed cases. The information pertaining to these 4 cases is reported in Table I. Based on Table I, the locations of actual and identified sources in the failed cases are highlighted in Figure 4. For example, for the first failed case in Table I, a periodic

perturbation with frequency 1.1033 Hz is injected into the system through the generator directly connecting to Bus 55, which is highlighted with a solid circle in Figure 4, whereas the identified source measurement is Bus 54 highlighted with a dash circle in Figure 4. As can be seen in the figure, the identified and actual source measurements are geographically close. Similar conclusions can be drawn from the remaining three failed cases listed in Table I. Therefore, even the failed cases from the proposed method can effectively narrow the search space.

TABLE I  
COMPARISON BETWEEN INACCURATE RESULTS AND GROUND TRUTH IN THE IEEE 68-BUS SYSTEM

Case #	Bus # (Identified)	Bus # (Truth)	Freq. (Hz)
1	54	55	1.1033
2	54	55	1.1504
3	59	58	1.2855
4	59	58	1.2892

### B. Performance Validation of the Source Localization Method in the WECC 179-bus System

This subsection leverages the open-source forced oscillation dataset [31] to validate the performance of the RPCA-based method. The offered dataset is generated via the WECC 179-bus power system [32] whose topology is shown in Figure 5(a). The procedure of synthesizing the data is reported in [32]. The available dataset includes 15 forced oscillation cases with single oscillation source, which are used to test the proposed method. In each forced oscillation case, the voltage magnitude measurements at all generation buses are used to construct the measurement matrix  $Y_t$  in (4), from the 10-second oscillatory data, i.e.,  $T_0 = 10$ . Then, the 15 measurement matrices are taken as the input for Algorithm 1, where the tunable parameter  $\xi$  is set to 0.0577 using the same reasoning as in Section V-A.

For the WECC 179-bus system, the proposed method achieved 86.67% accuracy. There are two failed cases listed in Table II. Next, we present how geographically close the identified FO sources are to the ground truth in the two seemingly incorrect cases. In Case FM-3, a sinusoidal perturbation with a frequency of 0.37 Hz is injected into the grid through the governor of the generator at Bus 77. In Figure 5 (b), Bus 77 is highlighted with a red solid circles. The source measurement identified by the proposed method is at Bus 65 which is highlighted by a red dash circle. As can be seen in Figure 5 (b), the identified FO source is geographically close to the actual source. A similar conclusion can be drawn for another failed case named “FM-6-2”, where the ground truth is Bus 79 while the identified source is at Bus 65. Again, even the seemingly wrong result can help system operators substantially narrow down the search space for FO sources.

## VI. CONCLUSION

In this paper, a purely data-driven but physically interpretable method is proposed in order to locate forced oscillation sources in power systems. The localization problem

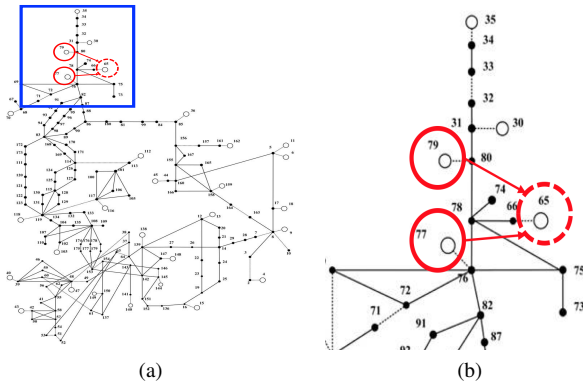


Fig. 5. WECC 179-bus power system [32]: (a) complete topology; (b) zoomed-in version of the area in blue box in the left figure.

TABLE II  
COMPARISON BETWEEN INACCURATE RESULTS AND GROUND TRUTH IN  
THE WECC 179-BUS SYSTEM

Bus # (Identified)	Bus # (Truth)	Case No.
65	77	FM-3
65	79	FM-6-2

is formulated as an instance of matrix decomposition, i.e., how to decompose the high-dimensional synchrophasor data into a low-rank matrix and a sparse matrix, which can be done using Robust Principal Component Analysis. Based on this problem formulation, an online localization algorithm is presented. The proposed algorithm does not require any information on system models nor grid topology, thus enabling an efficient and wide implementation for real-time operation. In addition, a possible theoretical interpretation of the efficacy of the algorithm is provided based on physical model-based analysis, highlighting the fact that the rank of the resonance matrix is at most 2. Future work will further examine the theoretical connection between the resonance-free components of PMU measurements and the sparse matrix in the RPCA formulation. We also plan to test this algorithm in much larger-scale realistic cases.

## REFERENCES

- [1] J. D. L. Ree, V. Centeno, J. S. Thorp, and A. G. Phadke, "Synchronized phasor measurement applications in power systems," *IEEE Transactions on Smart Grid*, vol. 1, no. 1, pp. 20–27, June 2010.
- [2] L. Xie, Y. Chen, and P. R. Kumar, "Dimensionality reduction of synchrophasor data for early event detection: Linearized analysis," *IEEE Transactions on Power Systems*, vol. 29, no. 6, pp. 2784–2794, Nov 2014.
- [3] T. Huang, N. Freris, P. R. Kumar, and L. Xie, "Localization of forced oscillations in the power grid under resonance conditions," in *52nd Annual Conference on Information Sciences and Systems (CISS)*, March 2018, pp. 1–5.
- [4] T. Huang, M. Wu, and L. Xie, "Prioritization of PMU location and signal selection for monitoring critical power system oscillations," *IEEE Transactions on Power Systems*, vol. 33, no. 4, pp. 3919–3929, July 2018.
- [5] M. Ghorbaniparvar and N. Zhou, "A survey on forced oscillations in power system," *CoRR*, vol. abs/1612.04718, 2016. [Online]. Available: <http://arxiv.org/abs/1612.04718>
- [6] C. Vournas, N. Krassas, and B. Papadias, "Analysis of forced oscillations in a multimachine power system," in *International Conference on Control*. IET, 1991, pp. 443–448.

- [7] A. Silverstein, "Diagnosing equipment health and mis-operations with PMU data," *Diagnosing Equipment Health and Mis-operations with PMU Data*, 2015.
- [8] S. A. N. Sarmadi, V. Venkatasubramanian, and A. Salazar, "Analysis of november 29, 2005 western american oscillation event," *IEEE Transactions on Power Systems*, vol. 31, no. 6, pp. 5210–5211, Nov 2016.
- [9] E. L. S. Maslennikov, B. Wang, "Locating the source of sustained oscillations by using PMU measurements." IEEE PES General Meeting, 2017.
- [10] P. B. Reddy and I. A. Hiskens, "Limit-induced stable limit cycles in power systems," in *IEEE Russia Power Tech*, June 2005, pp. 1–5.
- [11] K. R. Rao and L. Jenkins, "Studies on power systems that are subjected to cyclic loads," *IEEE Transactions on Power Systems*, vol. 3, no. 1, pp. 31–37, Feb 1988.
- [12] S. Maslennikov, "Detection the source of forced oscillations," Tech. Rep. [Online]. Available: <https://www.naspi.org/node/653>
- [13] S. A. N. Sarmadi and V. Venkatasubramanian, "Inter-area resonance in power systems from forced oscillations," *IEEE Transactions on Power Systems*, vol. 31, no. 1, pp. 378–386, 2016.
- [14] N. Zhou, M. Ghorbaniparvar, and S. Akhlaghi, "Locating sources of forced oscillations using transfer functions," in *IEEE Power and Energy Conference at Illinois (PECI)*, Feb 2017, pp. 1–8.
- [15] L. Chen, Y. Min, and W. Hu, "An energy-based method for location of power system oscillation source," *IEEE Transactions on Power Systems*, vol. 28, no. 2, pp. 828–836, 2013.
- [16] E. L. S. Maslennikov, B. Wang, "Dissipating energy flow method for locating the source of sustained oscillations," *International Journal of Electrical Power & Energy Systems*, pp. 55–62, 2017.
- [17] W. Bin and S. Kai, "Location methods of oscillation sources in power systems: a survey," *Journal of Modern Power Systems and Clean Energy*, vol. 5, no. 2, pp. 151–159, 2017.
- [18] S. C. Chevalier, P. Vorobev, and K. Turitsyn, "Using effective generator impedance for forced oscillation source location," *IEEE Transactions on Power Systems*, vol. 33, no. 6, pp. 6264–6277, Nov 2018.
- [19] S. Chevalier, P. Vorobev, and K. Turitsyn, "A Bayesian approach to forced oscillation source location given uncertain generator parameters," *IEEE Transactions on Power Systems*, pp. 1–1, 2018.
- [20] "Var-501-wecc-3power system stabilizer," Tech. Rep. [Online]. Available: <https://www.wecc.biz/Reliability/VAR-501-WECC-3.pdf>
- [21] T. Huang, B. Satchidanandan, P. R. Kumar, and L. Xie, "An online detection framework for cyber attacks on automatic generation control," *IEEE Transactions on Power Systems*, vol. 33, no. 6, pp. 6816–6827, Nov 2018.
- [22] H. Ye, Y. Liu, P. Zhang, and Z. Du, "Analysis and detection of forced oscillation in power system," *IEEE Transactions on Power Systems*, vol. 32, no. 2, pp. 1149–1160, March 2017.
- [23] R. Diestel, *Graph theory (Graduate texts in mathematics)*. Springer Heidelberg, 2005, vol. 173.
- [24] J. H. Chow and K. W. Cheung, "A toolbox for power system dynamics and control engineering education and research," *IEEE Transactions on Power Systems*, vol. 7, no. 4, pp. 1559–1564, 1992.
- [25] E. J. Candès, X. Li, Y. Ma, and J. Wright, "Robust Principal Component Analysis?" *Journal of the ACM (JACM)*, vol. 58, no. 3, p. 11, 2011.
- [26] Z. Lin, M. Chen, and Y. Ma, "The Augmented Lagrange Multiplier method for exact recovery of corrupted low-rank matrices," *arXiv preprint arXiv:1009.5055*, 2010. [Online]. Available: <https://arxiv.org/abs/1009.5055>
- [27] X. Wang and K. Turitsyn, "Data-driven diagnostics of mechanism and source of sustained oscillations," *IEEE Transactions on Power Systems*, vol. 31, no. 5, pp. 4036–4046, Sept 2016.
- [28] M. A. Khan and J. W. Pierre, "Detection of periodic forced oscillations in power systems using multitaper approach," *IEEE Transactions on Power Systems*, pp. 1–1, 2018.
- [29] J. Follum and J. W. Pierre, "Detection of periodic forced oscillations in power systems," *IEEE Transactions on Power Systems*, vol. 31, no. 3, pp. 2423–2433, May 2016.
- [30] H. Bevrani, M. Watanabe, and Y. Mitani, *Power system monitoring and control*. John Wiley & Sons, 2014.
- [31] S. Maslennikov, X. Xu, K. Sun, and B. Wang, "Test cases library of power system sustained oscillations," ISO-NE and UTK, Tech. Rep. [Online]. Available: <http://web.eecs.utk.edu/~7Ekaisun/Oscillation/simulatedcases.html>
- [32] S. Maslennikov, B. Wang, Q. Zhang, a. Ma, a. Luo, a. Sun, and E. Litvinov, "A test cases library for methods locating the sources of sustained oscillations," in *IEEE Power and Energy Society General Meeting (PESGM)*, July 2016, pp. 1–5.